

ORIGINAL ARTICLE

Molecular simulations of the structure and thermal transport of high alumina aluminosilicate molten core glass fiber

Bennett Greenberg¹  | Stephen H. Garofalini² 

¹Department of Physics and Astronomy, Rutgers University, Piscataway, New Jersey

²Department of Materials Science and Engineering, Interfacial Molecular Science Laboratory, Rutgers University, Piscataway, New Jersey

Correspondence

Stephen H. Garofalini, Department of Materials Science and Engineering, Rutgers University, Piscataway, NJ.
Email: shg@rutgers.edu

Abstract

The atomistic structure and phonon transport in aluminosilicate glasses made via an interfacial mixing model of the Molten Core process were studied using molecular dynamics simulations. In the simulations, silica glass was brought in contact with different size alumina crystals (to afford core glasses with 4, 18, 24, 29, and 41 mole% alumina concentrations), followed by a melt-quench process to enable mixing of the phases. The atomistic structure of the resulting glasses and radius of gyration calculations of resultant Al-O-Al connected clusters were evaluated. Variation in the 1-dimensional thermal transport in each glass was also determined and showed that increased alumina concentration in the glasses resulted in increased transport of thermal energy. Results of the structural analyses showed a double peak in the Al-Al pair distribution function, with the short-distance peak indicative of edge-sharing Al-O-Al-O bonding and a longer distance peak of Al-O-Al bonding that is not indicative of edge-sharing structures. The ratio of the first Al-Al peak to the second Al-Al peak varied inversely with the thermal transport behavior. An increased radius of gyration of Al-O-Al connectivity occurred with increasing alumina concentration, providing a mechanism for the increased thermal transport. Nanosegregation was also observed. Interconnectivity between Al ions created isolated Al-O-Al bonded clusters at low alumina concentrations with lower thermal transport than the high alumina glasses, whereas the latter showed a percolated network of Al-O-Al bonds that increased thermal transport.

KEYWORDS

atomistic simulation, glass, structure, thermal properties

1 | INTRODUCTION

Traditional optical fibers work well for low-energy telecommunications and laser systems, but there is a need for optical fibers that can transmit high-energy light waves without a significant amount of Brillouin scattering or Brillouin gain.¹ Previous studies have shown that optical fibers with a core consisting of a mixture of SiO₂ and Al₂O₃ have properties that allow the fiber to have a significantly reduced Brillouin gain coefficient,² which should allow for narrow-linewidth high-power lasers.³ Unfortunately, the

traditional chemical vapor deposition (CVD) method of making optical fibers limits the amount of alumina that can be in the core of the optical fiber to about 12 weight% (8 mole%), resulting in optical fibers that still allow for a significant and costly amount of Brillouin gain.^{4,5} Fortunately, another method for making optical fibers was developed called the molten core approach.^{6,7} Cr:YAG and YAG (yttrium aluminum garnet) are 2 examples initially studied as the core crystalline materials in the silica cladding following by fiber drawing.^{8,9} In this approach, a precursor crystalline core material is set inside of the silica cladding,

followed by the fiber drawing at temperatures sufficiently high to melt the crystalline core. A portion of the surrounding silica cladding dissolves into the core, forming a silicate glass based on the composition of the core crystalline starting material. As an example relevant to this paper, this method has allowed incorporation of over 50% alumina in the aluminosilicate glassy core after fiber drawing.⁶ Use of a corundum core in the molten core approach for making the fiber was shown to reduce Brillouin scattering significantly.^{6,10,11} At the high draw temperature, the corundum core is molten and reacts with the silica cladding at the core/cladding interface, allowing the silica to penetrate throughout the core. Because of the significantly excess volume of the cladding with respect to the core volume, a core/cladding fiber is retained after drawing. The high temperature of the melt can be above the consolute point of a 2-liquid immiscibility and combination of the rapid cooling inherent in the draw process and the increased viscosity of the constituents can prevent phase segregation (although the cooling rate is much slower than the required cooling rate to prevent phase separation in a high alumina aluminosilicate glass).¹⁰ Additional benefits of using the molten core approach for compositions other than just adding alumina have been previously discussed.^{6,7,12}

Despite all of the accomplishments of these novel aluminosilicate optical fibers made using the Molten Core method, what is lacking is an understanding of the atomistic structure⁶ of these glasses. Here, we present results of molecular dynamics (MD) simulations of the mixing of crystalline alumina and amorphous silica in the molten state, quenched to create an aluminosilicate glass, followed by analysis of the resultant structure and the vibrational transfer of energy for different compositions.

2 | COMPUTATIONAL PROCEDURE

For this study, the molecular dynamics (MD) simulations employed an all-atom multibody potential was used that has been shown to successfully reproduce the structure and surface energies of α - and γ -alumina and vitreous silica glass, and multicomponent silicate glasses and intergranular amorphous aluminosilicate films between alumina crystal surfaces.¹³⁻¹⁶ The potential involves 2-body and 3-body terms:

The 2-body interactions are calculated using the following form,

$$V_{ij}^{2\text{-body}} = A_{ij} \exp\left(\frac{-r_{ij}}{\rho_{ij}}\right) + \left(\frac{z_i z_j e^2}{r_{ij}}\right) \operatorname{erfc}\left(\frac{r_{ij}}{\beta_{ij}}\right) \quad (1)$$

and the optimal values of the parameters A_{ij} , β_{ij} , and ρ_{ij} for each pair were determined in previous work. z_i and z_j

represent the full charge of the ions i and j , and e represents the elementary charge. r_{ij} denotes the separation between the ions i and j .

The 3-body term is included to account for the partial covalency of Si-O and Al-O bonding. These interactions are described as:

$$\text{If } r_{ij} < R_{ij} \text{ and } r_{ik} < R_{ik},$$

$$V_{jik}^{3\text{-body}} = \lambda_{ij}^{1/2} \lambda_{ik}^{1/2} * \exp\left[\frac{\gamma_{ij}}{(r_{ij} - R_{ij})} + \frac{\gamma_{ik}}{(r_{ik} - R_{ik})}\right] \Theta_{jik}, \quad (2)$$

else,

$$V_{jik}^{3\text{-body}} = 0 \quad (3)$$

The angular component Θ_{jik} for Si/Al-O-Si/Al/and O-Si-O is given by,

$$\Theta_{jik} = \left(\cos \theta_{jik} - \cos \theta_{jik}^0\right)^2 \quad (4)$$

and the angular component for O-Al-O is given by,

$$\Theta_{jik} = \left(\left(\cos \theta_{jik} - \cos \theta_{jik}^0\right) \sin \theta_{jik} \cos \theta_{jik}\right)^2 \quad (5)$$

where θ_{jik} is the angle formed by the ions j , i , and k with the ion i as the vertex. The θ_{jik}^0 term in each equation is 109.45° and is designed to promote, but not restrict, tetrahedral bonding. The additional sine and cosine terms enable Equation 5 to have multiple minima that add more flexibility and reliability for Al bonding in tetrahedral and octahedral states. Similar to the 3-body term on the Si, which is tetrahedral but allows for 5-coordinated Si as a reaction intermediate that can exist post quench in simulations and experiment,¹⁷⁻¹⁹ the Al 3-body also allows for 5-coordinated Al to form at small concentrations. In recent simulations of multicomponent silicate glasses, a small concentration of 5-coordinated Al is observed.²⁰ Parameters are the same as previously published.^{21,22}

These molten core (MC) MD simulations involved placing amorphous silica in contact with different size α -Al₂O₃ crystals. System sizes are given in Table 1. Initially, the amorphous silica was melted at high temperature for 500 000 time steps at 8000K while keeping the alumina crystal frozen so as to attain the crystal/glass interface. This was followed by melting the whole system (both phases) at high temperature given in Table 2 to allow for intermixing of the phases to create a molten aluminosilicate liquid, followed by quenching through intermediate temperatures to form an aluminosilicate glass. Periodic boundary conditions are employed in all 3 dimensions. The time step used in the simulations was 1 fs. The alumina crystals were sized to allow for the resultant glasses to contain 4 mole%, 18 mole%, 29 mole%, and 41 mole% of alumina. The latter 3 compositions were somewhat similar to compositions presented by

TABLE 1 Compositions, number of atoms, and systems sizes in X, Y, and Z (in Å), and expansion in Z

Composition	No. of atoms	X	Y	Z	Expansion (z)
4 mol% Al ₂ O ₃	47142	53.66	42.309	337.28	2.90%
18 mol% Al ₂ O ₃	48000	58.258	50.352	269.6	15.70%
24 mol% Al ₂ O ₃	49998	57.685	50.172	283.6	24.38%
29 mol% Al ₂ O ₃	48300	52.802	49.891	301	30.60%
41 mol% Al ₂ O ₃	48000	56.709	49.06	274.34	41.30%

TABLE 2 Melt/quench process. P_i gives the pressure in the i dimension. Below 4000K, constant pressure in all dimensions is used

Temperature	Time	Pressure
8000K	4000 ps	P _z =10000 atm, Const. x & y
7000K	100 ps	Const. V
6000K	75 ps	Const. V
5000K	75 ps	Const. V
4000K	200 ps	Const. V
3500K	200 ps	P _x =P _y =P _z =1 atm
3000K	200 ps	P _x =P _y =P _z =1 atm
2000K	75 ps	P _x =P _y =P _z =1 atm
1000K	50 ps	P _x =P _y =P _z =1 atm
298K	25 ps	P _x =P _y =P _z =1 atm

Dragic et al¹⁰ via the molten core process. The 4 mole% composition was meant to represent the fiber core made by the traditional chemical vapor deposition method, although for this study it was created using the same simulated molten core approach as the other concentrations to ensure that any differences in its properties would be a result of the concentrations of alumina and silica, and not some consequence of the process. The 24 mol% system was added after consideration of Al-Al PDF data regarding the intensity of the first peak, so some other data were not deemed necessary. A second 41 mol% glass made via this molten core approach was also done to see the differences that might occur. The starting configuration was the same as the first 41 mol% glass except that the initial high temperature run of the silica alone in contact with the crystal was run for twice the time to create a different starting silica glass structure in contact with the alumina crystal.

An additional study using a classic MD simulation approach for making a glass was also used for one of the molten core compositions. In this classic simulation process, the ions consistent with the 41 mol% system were randomly distributed throughout a volume that would end up at 298K with a density similar to the molten core

simulated system. The initial distribution of ions was such that no 2 ions were too close in distance. This glass is labeled as the Melt Quench (MQ) glass, to distinguish it from the “Molten Core” glasses. (Of course, both types of glasses went through a melt quench process, but the initial starting configurations were completely different.) The structure of this resultant MQ glass and thermal transport were analyzed and compared to that for the 41 mol% molten core glass.

Structural analyses of the glasses were obtained via radial, pair and total distribution functions (RDF, PDF, and T(r), respectively) where T(r) gives number of neighbors as a function of distance. Al rich clusters were observed in the aluminosilicate glasses and cluster sizes were analyzed using calculation of the radius of gyration. A cluster was determined by the connectivity of the Al (via the O) using a program that finds all aluminum atoms within a cutoff of any other Al atom in the cluster. Two cutoffs were used: one at 2.85 Å (the location of the first minimum of the double peak in the Al-Al PDF indicative of edge-sharing) and a second cutoff at 3.63 Å (the minimum after the second peak in the Al-Al PDF indicative of all Al-O-Al structures). The program starts with an aluminum atom to create a potential cluster, then loops through the rest of the aluminum atoms in the system. If it finds one within the cutoff, the new atom is added to the cluster and marked as used. The program then goes back to loop over all unused aluminum atoms again to see if any are within the cutoff of any of the members of the existing cluster. Once a cluster is complete (no more Al atoms are within the cutoff of any of the atoms in the cluster), the radius of gyration of the cluster is calculated.

To determine the vibrational transport of thermal energy along the z dimension (long dimension) of the simulated fiber core, a localized thermal pulse was imposed on a portion of the glass and the temperature change in a different section of each glass was analyzed. In this process, a small volume of atoms about 5 Å thick, from 0 to 5 Å in the z direction at one end of the glass was instantaneously heated up to 4000K using velocity rescaling of the atoms in that volume. This heating occurred for 20000 initial steps followed by 80 000 steps with no further equilibration. The rest of the glass was not re-equilibrated throughout the entire run and the temperature in a ~10 Å thick volume in the middle of the glass core in the long direction was then tracked as a function of time to see how the heat propagated through the system as a function of composition.

Observation of a dual-peak in the Al-Al pair distribution functions (PDFs) led to consideration of the cause of these 2 peaks. The short-distance peak is attributed to 2-membered Al-O-Al-O rings (edge-sharing) in the

resultant glasses, as discussed below, creating a short-range local structure that also exists in the crystalline corundum form.

3 | RESULTS

Figure 1A shows the starting configuration for the 18% alumina system, whereas Figure 1B shows the system after the molten core procedure. Clusters of Al (red) can be seen in Figure 1B (of course, these are not metallic clusters of Al, but rather with Al still bonded to O). Figure 1 shows that the crystal melts and mixes thoroughly with the silica.

Figure 2 shows the radial and pair distribution functions (RDF and PDF, respectively) for the 29 mol% Al_2O_3 glass as an example of the glass structure. The RDF in Figure 2A exhibits a first peak at 1.61Å, indicative of the Si-O first peak, with a shoulder at the longer distance side caused by the Al-O. Figure 2B shows the Si-O PDF, 2c shows the Al-O PDF, and 2d shows the O-O PDF. The Al-O PDF shows a shoulder at the longer distance side of the first peak, indicative of a dual spacing for Al-O bonds that will be addressed below regarding small alumina rings. The shoulder on the longer distance side of the first O-O peak in the O-O PDF is caused by the presence of the Al and increases with increasing alumina content.

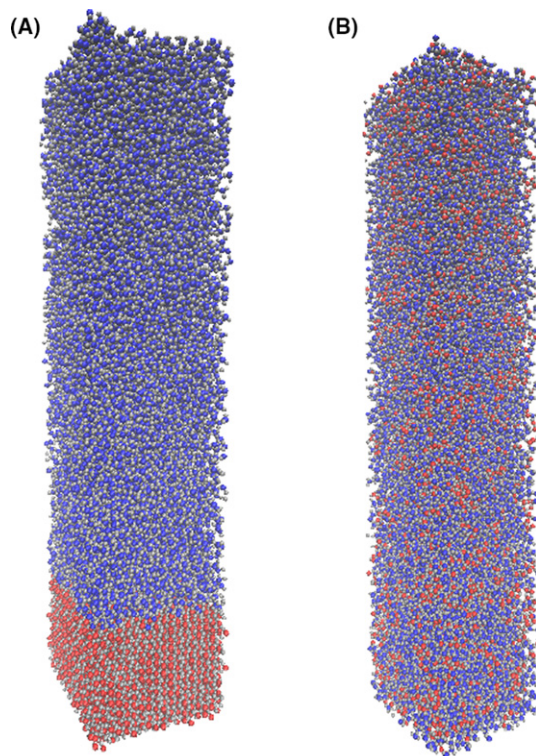


FIGURE 1 A, Initial pre-melt configuration of the 18% alumina system; B, post-melt/quench configuration. Al=red, Si=blue, O=gray

Figure 2E shows the Al-Al pair distribution functions (PDF) for the 29 mol% Al_2O_3 glass. The Al-Al PDF exhibits a double peak, with maxima at 2.70 Å and 3.21 Å and a minimum at 2.85 Å between them and a second minimum at 3.63 Å. This first peak in this double peak is a result of 2-membered rings caused by edge-sharing, in which the 2.70Å peak is between Al that share an oxygen edge as shown in the circle in Figure 3. Such edge sharing is seen in the $\alpha\text{-Al}_2\text{O}_3$ crystalline form containing 40% 2-membered rings. In their study of amorphous Al_2O_3 , Guiterrez et al²³ observed 2-membered rings at 9.1%. In our case, such 2-membered rings exist in the simulated aluminosilicate glasses, although, as shown below, larger scale connectivity between Al ions via oxygen that are not in 2-membered rings also exists and is indicative of Al-O-Al connectivity. A “cluster” of 2-membered rings may exist and will be shown below to be very small in size; larger scale nanosegregation of Al (in what might also be called “clusters”) involved in Al-O-Al connectivity without necessarily being in 2-membered rings also exists and dominates the structure. A distinction in the terminology of “clusters” used in the text will use “edge-clusters” to distinguish discussion of the 2-membered rings cluster from the nanosegregation of Al-O-Al bonding forming larger scale “Al-O-Al clusters”. Examples of this Al-O-Al connectivity will be shown below in subsequent figures.

A notable difference between systems of different compositions was the size of Al-O-Al clusters. Figure 4 shows the clustering of the alumina as a function of Al_2O_3 content for 3 of the systems via the groupings of the red Al ions. Clearly, with more alumina in the glasses, there is more connectivity between Al ions (via O). The size of the 2 types of clusters was determined using the radius of gyration of the clusters using 2 cut-off ranges for determining the type of clustering. Using 2.85Å as the cut-off radius would provide cluster sizes of the 2-membered (edge-sharing) Al-O-Al-O rings; using a cut-off of 3.63Å would include all Al-O-Al connections and Al-O-Al clustering. The average radius of gyration for the 10 largest edge-sharing clusters of 2-membered rings in each composition using the edge-sharing cutoff of 2.85Å varied from 1.4 Å in the 4 mole% system to 3.4 Å in the 41 mole% system and is shown in Figure 5A. The value of 1.4 Å in the 4 mole% system indicates that there are no or few “edge-sharing clusters”, since this radius would mean a diameter distance of 2.8 Å which would just mean Al-Al distances in single pairs in a 2-membered ring configuration. The largest cluster of 2-membered rings has a radius of ~5Å and is in the 41% composition, although, as the average radius for that glass shows, there is a rapid decrease in the other 9 largest edge-sharing clusters such that the average for the top 10 edge-clusters is only ~3.5Å.

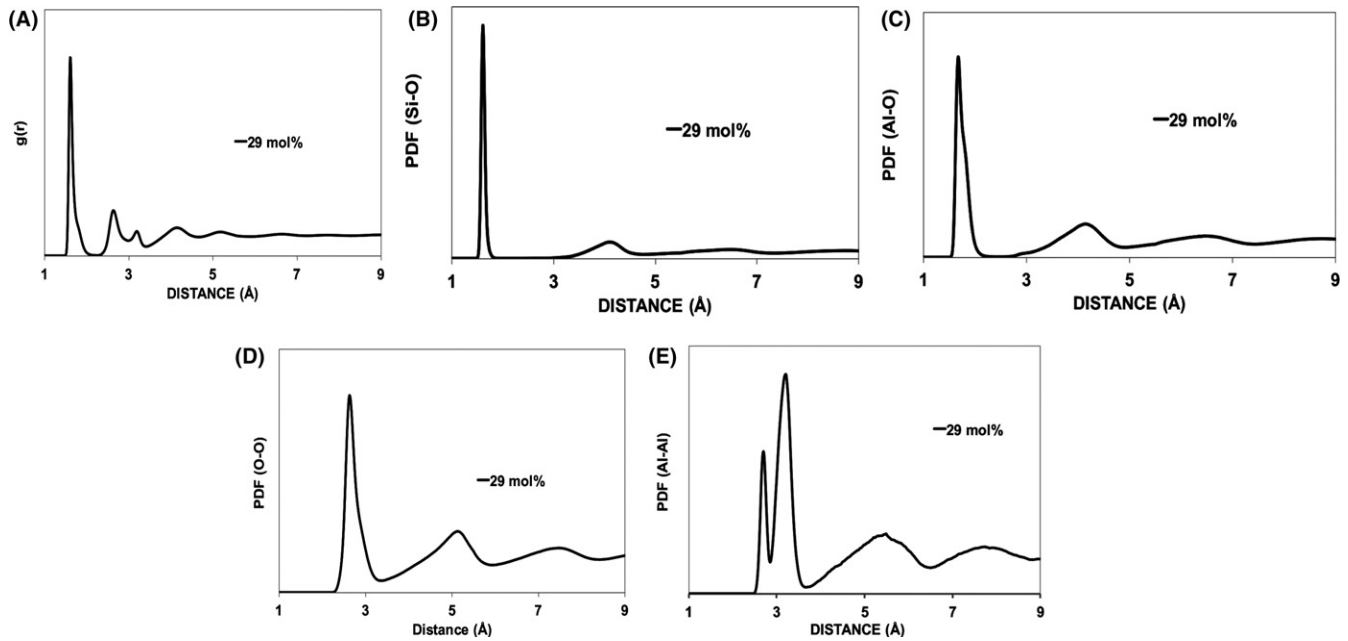


FIGURE 2 A, radial distribution function of the 29 mol% glass; B, Si-O pair distribution functions; C, Al-O pair distribution functions; D, O-O pair distribution functions; E, Al-Al pair distribution function for the 29 mol% glass showing a first peak associated with the edge-sharing Al-O-Al-O, with the second peak consistent with normal Al-Al distances in corner-shared tetrahedra

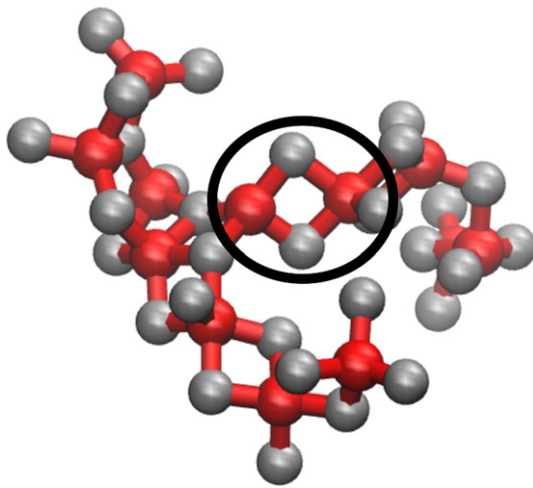


FIGURE 3 Edge sharing within an alumina cluster in the aluminosilicate glass. Red=Al, gray=O. Si and other O not drawn

The radius of gyration using a cut-off at 3.63\AA , which is at the end of the 2nd Al-Al first neighbor peak, provides information regarding all Al-O-Al connectivity, regardless of ring size. The average radius of the Al-O-Al clusters increases with increasing Al_2O_3 concentration. With the larger cut-off, the size and percent of Al atoms in the largest cluster varies as given in Table 3 and Figure 5B. At the 41 mol% compositions, almost all Al are within the largest cluster (96 and 97%), with the next largest size dropping below 10\AA radius. The 29 mol% glass has 85% of the Al ions in a single large Al-O-Al cluster. Contrastingly, the 18 mol%

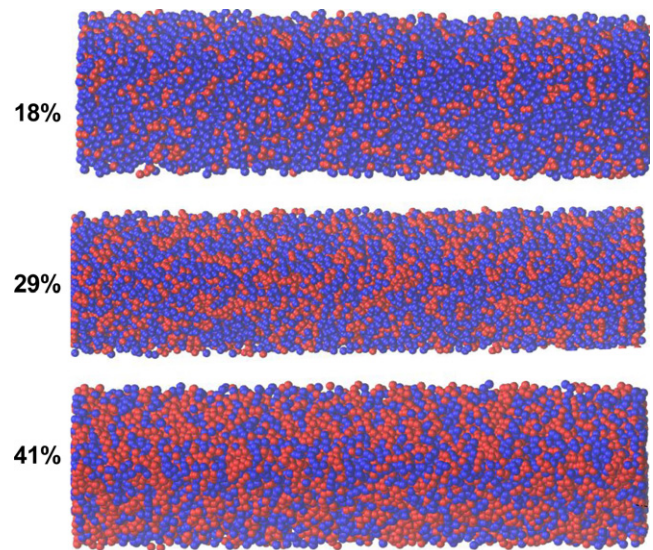


FIGURE 4 Snapshots of the 3 highest concentration alumina glasses after the melt-quench process. Red=Al, blue=Si (O not shown) showing the increased clustering of alumina with increased alumina concentration

glass has a much smaller maximum cluster size, with a much smaller percent of Al ions in that cluster; however, the next 8 smaller clusters are very similarly sized as the largest, indicating a large number of small Al-O-Al clusters that are not connected to each other. The 24 mol% glass has the next 10 clusters about 50% in size of the largest. Thus, the higher alumina concentration glasses have most of the Al ions

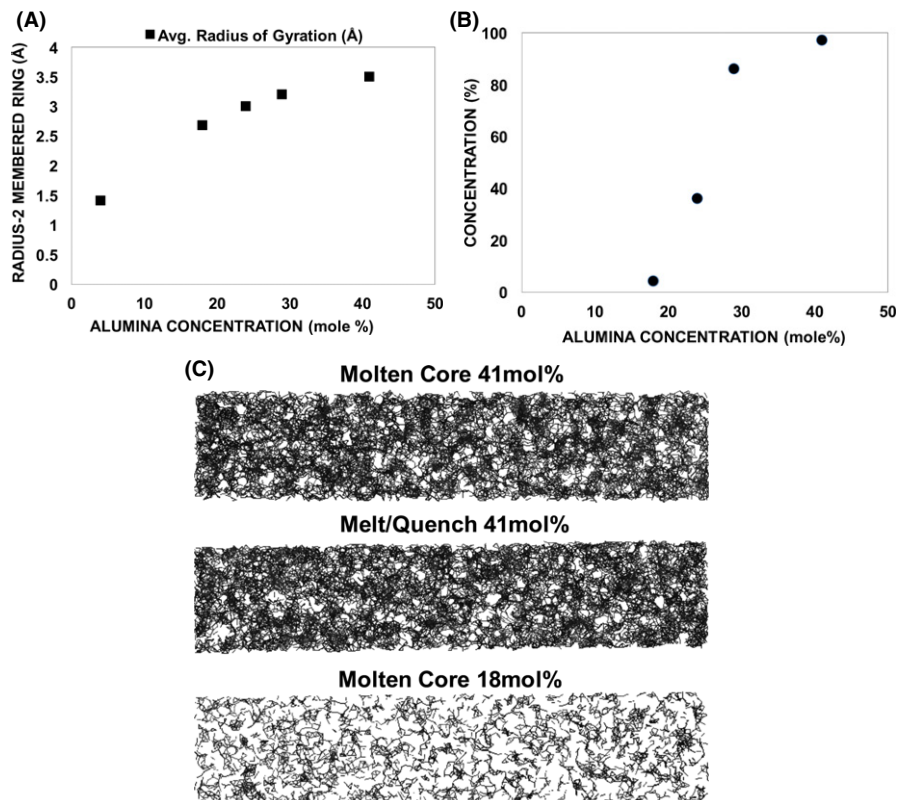


FIGURE 5 A, Average radius of gyration of top 10 largest alumina clusters of 2-membered rings as a function of alumina concentration using the 2.85 Å cutoff. B, Concentration of Al ions within the largest Al-O-Al cluster as a function of alumina concentration using the 3.63 Å cutoff. C, Snapshots of the Al-Al connectivity (via O) in the molten core 41mole% and 18 mol% and melt/quench 41 mol% glasses using the 3.6 Å cutoff

interconnected, forming a large percolated “Al-O-Al cluster” that is indicative of nanosegregation; the lower concentration glasses have a distribution of smaller clusters that are not interconnected to each other. An example of the Al-Al connectivity (via O) for the 41 mol% and 18 mol% glasses is shown in Figure 5C. The figure provides a snapshot of the molten core formed glasses at 41 mol% and 18 mol% (top and bottom of the figure) showing Al-Al (via connecting lines) within 3.6 Å of each other. The figure shows continuous connectivity among Al ions (via O) in the 41 mol% glass that is not present in the 18 mol% glass. Nanosegregation has apparently been observed in 3-component molten core glasses (J. Ballato, Personal Communication)

Figure 6A shows the coordination of O to Si and 6b shows the coordination of O to Al. The figures show that O is clearly attached to 2 Si in the 4 mole% Al₂O₃ glass,

TABLE 3 Largest size cluster of connected Al-O-Al using the 3.63 Å radius cut-off and percent of Al in the glass in this largest cluster

Composition [Al ₂ O ₃]	Al-O-Al Connected Clusters	
	Largest Radius (Å)	Al atoms in largest cluster (%)
18 mol%	19	4
24 mol%	46	36
29 mol%	94	85
41 mol%	90	97
41 mol% Standard Melt/Quench	93	96

with only a small percentage in 1 coordination. However, with increasing Al₂O₃ in the glass, there is a decrease in the concentration of O attached to 2 Si and an increase in the concentration of O with no Si neighbors or 1 Si neighbor. These changes in O attached to Si are compensated by the connectivity of the O to Al, as seen in Figure 6B. At the 4 mole% Al₂O₃ glass, the O have predominately no Al as first neighbors, but with increasing Al₂O₃ in the glasses, this decreases and is compensated with an increase in the O with 1 or 2 or 3 Al neighbors. Such changes in the O-Al coordination is approaching a more crystalline-like structure, as previously evidenced with the edge sharing of Al-O connectivity similar to α-Al₂O₃, but this is highly random and not indicative of crystallinity. The Si are all 4 coordinated in the glasses; the Al-O coordination numbers (CN) are shown in Table 4 showing a predominance of Al in 4 coordination, with some 3 CN, few 5 CN and no 6 CN. The table also shows the O coordination to Si or Al, with O in predominantly 2-fold coordination to the cations, but with an increasing concentration of 3-coordinated O with higher Al concentration. Such 3-coordinated O can be seen in the 2-membered rings of Al in Figure 3.

Figure 7 shows combinations of SiOSi, SiOAl, and AlOAl bonds on bridging oxygen as a function of Al₂O₃ in the glasses, showing the decrease in SiOSi triplets and significant increase in AlOAl with increasing Al₂O₃. This change shows a greater association of the Al ions with other Al ion, consistent with the effects of nanosegregation.

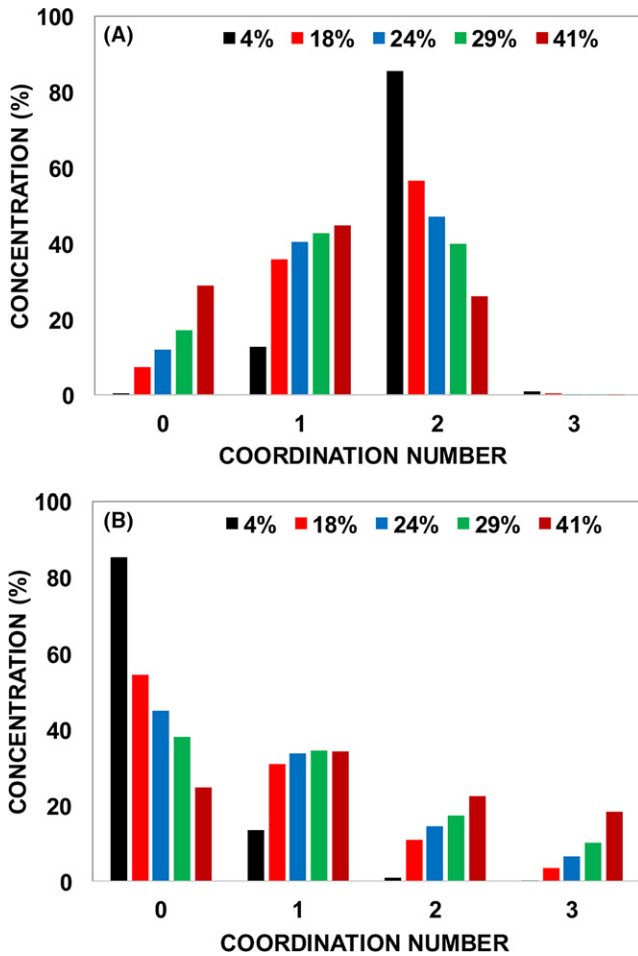


FIGURE 6 A, Coordination number of O—Si (number of Si attached to O); B, Coordination number of O—Al (number of Al attached to O)

TABLE 4 Al-O coordination and O-(Si,Al) coordination; the Si are all 4 coordinated to O

Composition	Al CN 3	Al CN 4	Al CN 5	Al CN 6
18 mol%	18	81	1	0
24 mol%	15	84	1	0
29 mol%	13	85	2	0
41 mol%	9	88	3	0
	O CN 1	O CN 2	O CN 3	O CN 4
18 mol%	0	87	13	0
24 mol%	0	82	18	0
29 mol%	0	78	22	0
41 mol%	0	68	32	0

3.1 | Phonon-like transport

Incorporation of alumina into silica has been shown to increase the acoustic velocity.²⁴ Since Brillouin scattering is affected by vibrations and phonon transport, altering

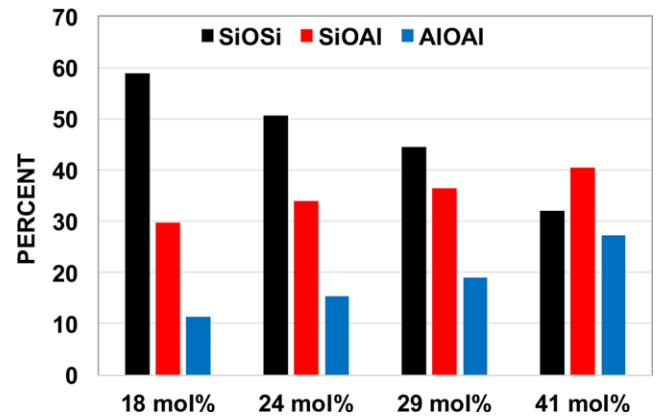


FIGURE 7 Bridging oxygen combinations as a function of alumina content in the glasses showing the decrease in SiOSi and significant increase in AlOAl with increasing alumina

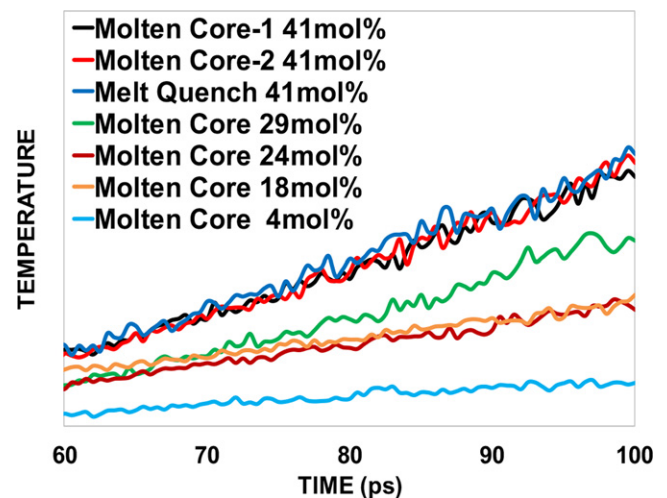


FIGURE 8 Change in the temperature of the central part of the glasses as a function of time over the final 40 ps showing that with more alumina, there is a more rapid transfer of thermal energy. Also shown is the second molten core run at 41 mol% and the standard melt-quench 41 mol% glass, showing that the results are not dependent upon the glass-forming procedure

polarizability, thermal excitement of atoms in a section of the glasses was used to evaluate transport of this energy via thermal transport through the glass. Figure 8 shows the change in temperature of a section in the middle of the glass as a result of heating a small section of glass atoms at the 0-5Å location in the z-dimension (the long dimension in Figure 1). Because of periodic boundaries, this heated section caused energy transport from both the bottom of the glass in z as well as from the top of the glass in z. Hence, the change in temperature in the middle of the glass was used as a measure of this transport as a function of composition. The temperature was sufficiently low that no significant diffusion of ions occurred.

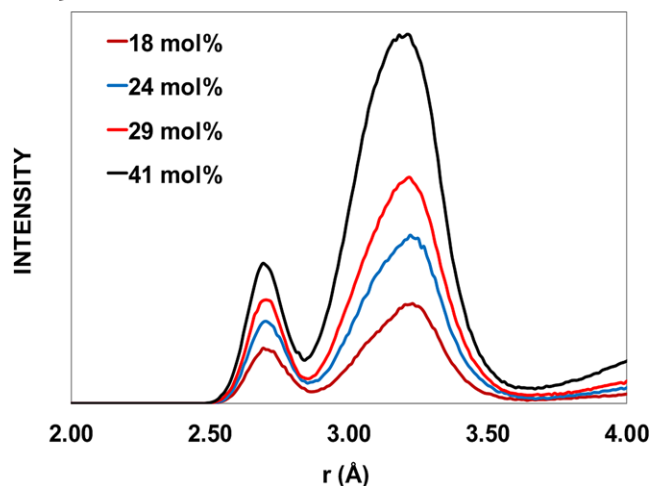


FIGURE 9 Al-Al total distribution intensity ($T(r)$) as a function of composition. The first to second peak area ratios are calculated from these curves

TABLE 5 Ratio of the first Al-Al peak area to the second Al-Al peak area in $T(r)$ for the different glass compositions

Glass	Ratio
18 mol%	0.28
24 mol%	0.24
29 mol%	0.22
41 mol%	0.18
41 MQ NVT	0.24

Figure 8 clearly shows that with increasing the Al_2O_3 content in the glasses there is a more rapid transport of thermal energy through the glass after 100 ps. The 4 mol% glass is clearly separated from the 18 and 24 mol% glasses, which are separated from the 29 mol% glass, which is separated from the 41 mol% glasses. This is consistent with the observed effect of adding alumina to silica glass on acoustic velocity.²⁴ It may also imply less Brillouin scattering with increased Al_2O_3 in the glasses, as evidenced in the experimental data from the Molten Core glasses.

The interesting structure observed in these simulations is the formation of Al-O-Al-O edges associated with the first Al-Al peak shown in Figure 2E. Calculation of the number of Al neighbors as a function of distance, giving the total distribution function $T(r)$, is given in Figure 9 as a function of composition. Using $T(r)$ shows the increase in the total number of Al-Al pairs in the first 2 peaks shown in Figure 9, consistent with the increase in the AlOAl concentration shown in Figure 7. An interesting feature in Figure 9 has to do with the ratio of these 2 peaks. The ratio of the first peak area to the second peak area is given in Table 5 showing that

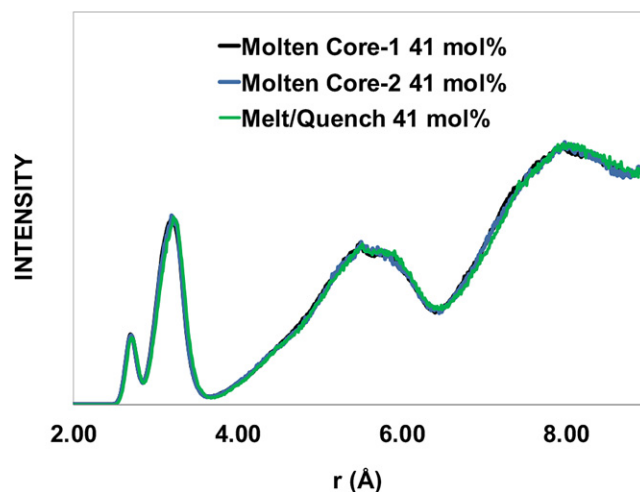


FIGURE 10 Al-Al pair distribution function for the 2 different starts 41 mole% glass formed by the process of melting the alumina crystal in contact with silica used in this paper (Molten Core) versus the standard melt/quench process used in many MD simulations of starting with a random distribution of ions followed by the same melt/quench procedure presented in Table 2. Results show that the Al-Al structure is almost exactly the same with either approach, resulting in the same thermal transport behavior for each of these 3 glasses (figure 8)

this ratio decreases with increasing alumina concentration. The change in this ratio is inversely related to the increase in thermal transport shown in Figure 8.

The anticorrelation between the 2-membered rings and phonon transport might imply that their presence impedes phonon transport. However, this would contradict the behavior in the crystalline form, where phonon transport is relatively high based on its low attenuation¹⁰ and there are a large number of these 2-membered rings in corundum, as stated above.

A more obvious link between the increased thermal transport with alumina content is the size and number of Al ions in the Al-O-Al clusters given in Table 3. The 4 mol% glass has essentially no Al clusters and acts as a potential baseline in Figure 8. With the 18 and 24 mol% glasses show similar thermal transport increase since their Al-O-Al clusters are not connected in a percolated network. The 29 mol% glass shows a larger increase in thermal transport, but only has 85% of the Al ions connected. With the 41 mol% glasses, Al-O-Al connectivity above 96% shows the highest thermal transport.

As mentioned above, 2 additional glasses with 41 mol% alumina were made: a second glass made via the molten core approach (alumina crystal initially in contact with silica glass) and a glass made via the standard MD simulation melt-quench approach (ions randomly distributed in the volume as the starting configuration). The Al-O-Al bonds (Al-Al distance below 3.63 Å) for the 41 mol% molten core and melt quench glasses are shown in Figure 5C (top

and center). The overall structures are very similar. The radius of gyration of each new glass is the same as found for the original 41 mol% glass. Figure 10 shows the Al-Al total correlation function for the 2 molten core glasses as well as that made via the standard melt-quench method. Results show that there is no difference between the 2 molten core glasses with each other or with that made by the standard method. The transport in thermal energy of these 2 additional glasses is included in Figure 8, also showing no difference between the different formation methods. This indicates that the simulated molten core method would generate a glass similar to the standard simulation melt-quench method.

4 | CONCLUSIONS

Increasing the alumina concentration in the aluminosilicate glasses has a significant effect on the concentration of Al-O-Al bonding and enhanced thermal transport. Evaluation of the rate of transport of thermal energy through the different glasses showed an increased rate for those glasses with a higher alumina concentration and may be consistent with the more effective reduction of Brillouin scattering and gain observed in the high alumina glasses made via the Molten Core method.¹⁰

The aluminosilicate glasses studied here have a split Al-Al PDF first peak, with the short-distance peak indicative of edge-sharing Al-O-Al-O 2 membered rings, similar to that observed in α -Al₂O₃ and a longer distance peak consistent with Al-O-Al bonds not at edges. These edge-sharing groups are interconnected to a maximum radius size of 5 Å in the highest Al concentration glass. The ratio of the first Al-Al peak area to the second Al-Al area showed an inverse relation to the rate of thermal transport in the glasses. This ratio indicates the ratio of the concentration of the edge-sharing Al-O-Al-O structure to that of normal Al-O-Al connectivity.

Using the larger radial cutoff that includes both the first and second Al-Al peaks for the radius of gyration calculation, much larger groups of Al-O-Al connectivity occurs. The 41 mol% Al₂O₃ glasses exhibit significant Al-O-Al connectivity throughout the bulk, as nearly all of the aluminum atoms in the bulk (96-97%) are connected through nearest second neighbors (oxygen being the first nearest neighbor). This apparent nanosegregation percolates throughout the whole glass, enhancing the overall thermal transport. Meanwhile, in the 24 and 18 mol% Al₂O₃ glasses, there is not a continuous network of Al-O-Al clusters throughout the whole glass, which decreases the thermal transport. The 29 mol% system fits between these 2 ranges both in thermal transport and percent of Al ions in Al-O-Al connectivity.

The results of the thermal pulse simulations confirm that the atomistic structure of aluminosilicates with higher alumina concentrations make them inherently better at transmitting phonons than those with lower alumina concentrations. The connectivity of the Al-O-Al bonding provides more rapid paths for vibrational transport that are not available in the silica portion of the glasses.

ORCID

Bennett Greenberg  <http://orcid.org/0000-0002-4922-1934>

Stephen H. Garofalini  <http://orcid.org/0000-0003-1718-2034>

REFERENCES

- Richardson D, Nilsson J, Clarkson W. High power fibre lasers: current status and future perspectives. *J Opt Soc Am B*. 2011;27: B63-B92.
- Davis T, Vedam K. Photoelastic properties of sapphire (a-Al₂O₃). *J Appl Phys*. 1967;38:4555-4556.
- Jeong Y, Sahu JK, Payne DN, et al. Ytterbium-doped large-core fiber laser with 1.36 kW continuous-wave output power. *Opt Express*. 2004;12:6088-6092.
- Nassau K, Shiever J, Krause J. Preparation and properties of fused silica containing alumina. *J Am Ceram Soc*. 1975;58:461-61.
- Simpson JR, MacChesney JB. Optical Fibres With An Al₂O₃-Doped Silicate Core Composition. *Electron Lett*. 1983;19:261-262.
- Ballato J, Dragic P. Rethinking optical fiber: new demands, old glasses. *J Am Ceram Soc*. 2013;96:2675-2692.
- Ballato J, Dragic PD. Materials development for next generation optical fiber. *Materials*. 2014;7:4411-4430.
- Huang Y, Wang J, Lu Y, et al. Preform fabrication and fiber drawing of 300 nm broadband Cr-doped fibers. *Opt Express*. 2007;15:14382-14388.
- Ballato J, Hawkins T, Foy P, et al. On the fabrication of all-glass optical fibers from crystals. *J Appl Phys*. 2009;105:053110.
- Dragic P, Hawkins T, Morris S, et al. Sapphire-derived all-glass optical fibers. *Nat Photonics*. 2012;6:629-635.
- Dragic P, Ballato J, Morris S, et al. Pockels' coefficients of alumina in aluminosilicate optical fiber. *J Opt Soc Am B*. 2013;30:244-250.
- Cavillon M, Kucera C, Hawkins T, et al. A unified materials approach to mitigating optical nonlinearities in optical fiber: III. Canonical examples and materials road map. *Int J Appl Glass Sci*. 2018;1-24. <https://doi.org/10.1111/IJAG.12336>.
- Blonski S, Garofalini SH. Molecular Dynamics Study of Silica-Alumina Interfaces. *J Phys Chem*. 1996;100:2201-2205.
- Blonski S, Garofalini SH. Molecular Dynamics Simulations of a-alumina and g-alumina Surfaces. *Surf Sci*. 1993;295:263-274.
- Zirl DM, Garofalini SH. Structure of Sodium-Aluminosilicate Glasses. *J Am Ceram Soc*. 1990;73:2848-2856.
- Feuston BP, Garofalini SH. Empirical three-body potential for vitreous silica. *J Chem Phys*. 1988;89:5818-5824.

17. Garofalini SH. Molecular dynamics computer simulations of silica surface structure and adsorption of water molecules. *J Non-Cryst Solids*. 1990;120:1-12.
18. Feuston BP, Garofalini SH. Water-induced relaxation of the vitreous silica surface. *J Appl Phys*. 1990;68:4830-4836.
19. Stebbins JF, McMillan P. Compositional and temperature effects on five-coordinated silicon in ambient pressure silicate glasses. *J Non Cryst Sol*. 1993;160:116-125.
20. Garofalini SH, Ha MT, Urraca J. Simulations of the surfaces of soda lime aluminoborosilicate glasses exposed to water. *J Am Ceram Soc*. 2017;101:1135-1148.
21. Zhang S, Garofalini SH. Molecular dynamic computer simulations of the interface structure of calcium-alumino-silicate intergranular films between combined basal and prism planes of α - Al_2O_3 . *J Am Ceram Soc*. 2005;88:202-209.
22. Ha M-T, Garofalini SH. Local structure of network modifier to network former ions in soda-lime-alumino-borosilicate glasses. *J Am Ceram Soc*. 2017;100:563-573.
23. Gutierrez G, Johansson B. Molecular dynamics study of structural properties of amorphous Al_2O_3 . *Phys Rev B*. 2002;65:104202104202.
24. Dragic P, Ballato J, Ballato A, et al. Mass density and the Brillouin spectroscopy of aluminosilicate optical fibers. *Opt Matl Exp*. 2012;2:1641-1654.

How to cite this article: Greenberg B, Garofalini SH. Molecular simulations of the structure and thermal transport of high alumina aluminosilicate molten core glass fiber. *J Am Ceram Soc*. 2018;00:1–10. <https://doi.org/10.1111/jace.15471>